Earth and Planetary Science Letters 415 (2015) 47–53

Contents lists available at ScienceDirect

Earth and Planetary Science Letters

www.elsevier.com/locate/epsl

Seasonal dynamic thinning at Helheim Glacier

Suzanne L. Bevan [a,*], Adrian Luckman [a], Shfaqat A. Khan [b], Tavi Murray [a]

[a] Geography Department, College of Science, Swansea University, SA2 8PP, United Kingdom
[b] DTU Space, National Space Institute, Technical University of Denmark, Department of Geodesy, Kgs. Lyngby, Denmark

ARTICLE INFO

Article history:
Received 19 September 2014
Received in revised form 23 January 2015
Accepted 24 January 2015
Available online 9 February 2015
Editor: P. Shearer

Keywords:
TanDEM-X
Helheim Glacier
mass balance
glaciology
dynamics

ABSTRACT

We investigate three annual mass-balance cycles on Helheim Glacier in south-east Greenland using TanDEM-X interferometric digital elevation models (DEMs), bedrock GPS measurements, and ice velocity from feature-tracking. The DEMs exhibit seasonal surface elevation cycles at elevations up to 800 m.a.s.l. with amplitudes of up to 19 m, from a maximum in July to a minimum in October or November, concentrated on the fast-flowing areas of the glacier indicating that the elevation changes have a mostly dynamic origin. By modelling the detrended bedrock loading/unloading signal we estimate a mean density for the loss of 671 ± 70 kg m^{-3} and calculate that total water equivalent volume loss from the active part of the glacier (surface flow speeds >1 m day^{-1}) ranges from 0.5 km^3 in 2011 to 1.6 km^3 in 2013. A rough ice-flux divergence analysis shows that at lower elevations (<200 m) mass loss by dynamic thinning fully explains seasonal elevation changes. In addition, surface elevations decrease by a greater amount than field observations of surface ablation or surface-energy-balance modelling predict, emphasising the dynamic nature of the mass loss. We conclude, on the basis of ice-front position observations through the time series, that melt-induced acceleration is most likely the main driver of the seasonal dynamic thinning, as opposed to changes triggered by retreat.

1. Introduction

The Greenland Ice Sheet (GrIS) has been losing mass since the early 1990s; observational evidence is based on airborne (Krabill et al., 1999, 2000; Thomas et al., 2006) and satellite altimetry (Johannessen et al., 2005; Pritchard et al., 2009; Zwally et al., 2011a), satellite gravity anomaly experiments (Velicogna and Wahr, 2005; Chen et al., 2006; Velicogna, 2009) and flux-balance calculations (Rignot and Kanagaratnam, 2006; Rignot et al., 2008). An attempt to reconcile these methods arrived at a 1992–2011 mass loss rate of 142 ± 49 Gt a^{-1} (Shepherd et al., 2012). Loss rates have been increasing, and recently CryoSat-2 altimeter observations showed that over the 3 yr up to January 2014 volume loss rates were 2.5 times greater than between 2003 and 2009 (Helm et al., 2014). On an ice-sheet wide basis the ice-dynamical and surface mass balance (SMB) contributions to the change are roughly equal (van den Broeke et al., 2009; Khan et al., 2014).

Mass balance at the marine-terminating outlet glaciers of the GrIS, however, can be dominated at times by losses resulting from glacier acceleration (Howat et al., 2011). For example, between 2002 and 2005 peak speeds on Helheim Glacier, a large marine-terminating outlet glacier in south-east Greenland and the focus of this study, increased by almost 30% and the front retreated by 7.5 km (Howat et al., 2005; Luckman et al., 2006). Helheim has since slowed and readvanced (Howat et al., 2007; Murray et al., 2010) but is yet to recover its pre-retreat state (Bevan et al., 2012). Peak rates of thinning of 60 ± 13 m a^{-1} occurred between 2004 and 2005 on the lower part of the glacier (Stearns and Hamilton, 2007), with dynamic thinning evident between 2003 and 2007 on fast-flow (>100 m a^{-1}) regions penetrating 95 km up-glacier (Pritchard et al., 2009).

Ongoing mass loss from the GrIS is superimposed on a seasonal cycle in ice-sheet mass balance which is dominated by the SMB processes of winter accumulation and summer ablation (van den Broeke et al., 2009; Bamber et al., 2012). This cycle is also detected in time series of gravity anomalies from the GRACE system (Velicogna, 2009; Ewert et al., 2012; Wahr et al., 2013), and in the vertical displacement solutions to bedrock-located continuous Global Positioning System (GPS) receivers (Bevis et al., 2012). Seasonal loading/unloading of ice causes the Earth to respond elastically (Farrell, 1972), resulting in vertical elastic surface displacement of the crust (Wahr et al., 2013). The magnitude of the displacement is proportional to the mass of the load and inversely

* Corresponding author.
E-mail address: s.l.bevan@swansea.ac.uk (S.L. Bevan).

http://dx.doi.org/10.1016/j.epsl.2015.01.031

proportional to the distance between the load and the observing point (Nielsen et al., 2013).

The processes that concentrate long-term dynamic mass loss on the outlet glaciers also influence the seasonal mass-balance cycle, as meltwater and runoff can affect flow velocities (Andersen et al., 2010; Sole et al., 2011; Joughin et al., 2008), submarine melt (Motyka et al., 2003; Jenkins, 2011), and iceberg calving (O'Leary and Christoffersen, 2013). Supraglacial melt is able to rapidly reach the bed at elevations below 1000 m via the development of moulins and crevasses (Clason et al., 2014; Bartholomew et al., 2010, 2011), and once it enters the subglacial hydrologic system it can reduce the effective pressure at the ice-bed interface to promote faster sliding. For example, the onset of melt has been observed to cause early season flow acceleration on many glaciers in western Greenland (Sole et al., 2011; Ahlstrøm et al., 2013). Evidence of melt-enhanced flow for glaciers in the southeast is weaker, but small variations in daily summer surface velocity on Helheim Glacier in 2007 and 2008 were found to be strongly correlated with daily melt (Andersen et al., 2010). At marine-terminating outlet glaciers meltwater and runoff will eventually reach the fjord.

Once discharged to the fjord the melt-season runoff can amplify submarine melting by forming bouyant plumes (Jenkins, 2011). These plumes drive an estuarine circulation within the fjords which, combined with the shelf-forced intermediary circulation, have a strong impact on the stratification of water within the fjord (Sutherland et al., 2014). Frontal ablation and the nature of waters present within the fjord therefore both depend significantly on meltwater discharge (Sciascia et al., 2013).

The importance of submarine melt lies not only in the first-order process of frontal mass loss via melt but also on the potential impact on calving. Modelling has shown that submarine melt could lead to undercutting of an ice front and hence increase the rate of calving (O'Leary and Christoffersen, 2013), though a more recent study has shown that this might not be the case in a time-evolving stress field (Cook et al., 2014). Seasonal melt water may also directly affect calving rates via crevasse hydrofracture processes. Where a crevasse-depth calving criterion is used to model calving rates, rates have been shown to be highly sensitive to water depth within the crevasses (Cook et al., 2012). Both submarine melting and increased calving can lead to terminus retreat and a subsequent reduction in resistive stresses at the terminus. This force imbalance may result in faster ice-flow and glacier thinning which rapidly propagates upstream (Howat et al., 2005).

Thus meltwater reaching the bed and progressing to the fjord may cause an increase in ice flow through two mechanisms — reduced basal friction and reduced terminal backstress, both of which will lead to dynamic thinning of a glacier during the melt season. Backstresses at the terminus may also vary seasonally owing to the formation and clearance of an ice mélange within the fjord (Howat et al., 2010; Amundson et al., 2010). In this study we investigate these processes by employing an unprecedented series of interferometric digital elevation models (DEMs) from June 2011 to May 2014. Using these data we map the timing and distribution of seasonal ice loss over Helheim Glacier below 800 m a.m.s.l. (above mean sea level) through three annual cycles. We calculate volume change using the DEM time series and associate this with mass loss by considering GPS measurements of relative vertical bedrock displacements from 2011 to 2014 at a permanent site located a few hundred meters from the Helheim Glacier (Fig. 1). Feature tracking of ice-flow is used to consider the relative contributions of SMB and dynamic effects to the annual mass-balance cycle, and the importance of ice-front processes versus meltwater penetration in driving dynamic processes.

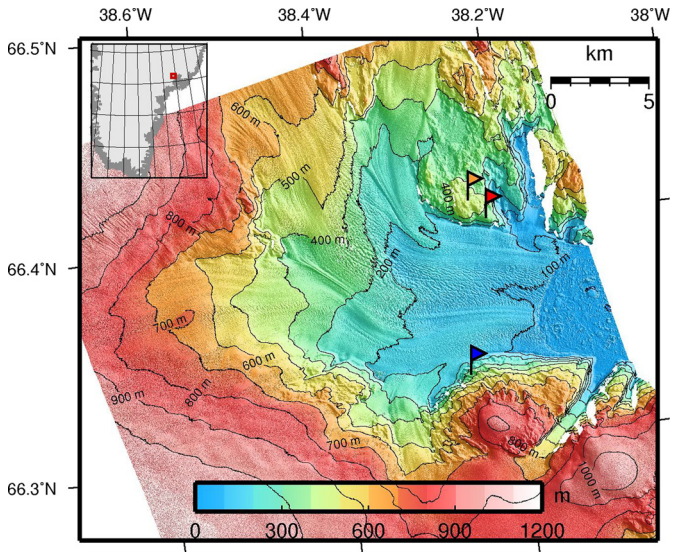

Fig. 1. Shaded digital elevation model for 02/07/2013. The orange flag marks the location and height for the ground control point (468.6 m), the blue flag the validation height point (347.1 m). The red flag marks the location of the GPS bedrock measurements. (For interpretation of the references to color in this figure legend, the reader is referred to the web version of this article.)

2. Methodology and data

2.1. Surface elevation

Synthetic Aperture Radar (SAR) data from the TanDEM-X satellite system were used to generate a series of DEMs of the lower portion of the Helheim Glacier catchment. The TanDEM-X mission is a public/private partnership between the German Aerospace Center (DLR) and EADS Astrium GmbH to generate a highly accurate consistent global DEM (Krieger et al., 2013). We use GAMMA Remote Sensing software to generate interferometric DEMs using the bistatic stripmap mode Co-registered Single look Slant range Complex products (CoSSCs). These experimental data are available over Helheim Glacier from June 2011 to May 2014 and have a spatial resolution of approximately 2 m which we multilook by a factor of 4. We rely solely on the provided orbital vector data to geolocate the images and to calculate the phase scaling. The DEMs are tied in the vertical dimension using a ground control point from the Danish Geodata Agency (http://gst.dk/emner/landkort-topografi/groenland/ground-control-greenland/, July 2014). The control point is at an elevation of 468.55 m above mean sea level in the GR96 datum system with a second point (347.10 m) used as a validation point (Fig. 1). All elevations quoted in this work will be in the GR96 datum system. The main error sources in generating interferometric DEMs from TanDEM-X data include errors in orbit or baseline information, unwrapping, and geolocation and orthorectification; only DEMs with less than a 2.5 m error relative to the validation point are included in this analysis. Estimates of orbit accuracies (Krieger et al., 2013) suggest that we cannot expect relative elevation accuracies better than 2 m.

Volume changes are calculated by differencing DEMs, only including ice-covered areas down to the most retreated frontal position. Area-mean surface elevation changes are calculated by dividing volume changes by the relevant area.

2.2. Surface velocity

We used TanDEM-X and earlier TerraSAR-X image pairs to measure surface velocities based on feature tracking (Strozzi et al.,

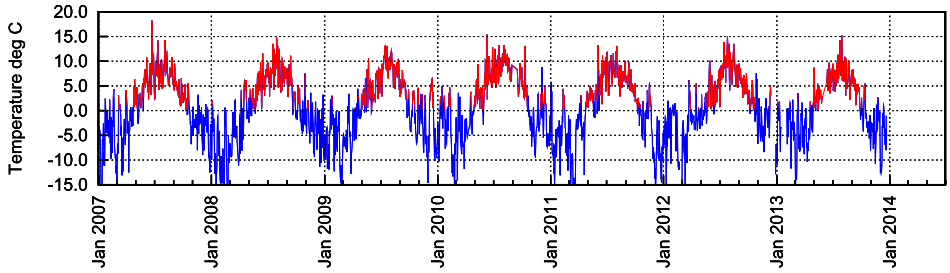

Fig. 2. 12z air temperatures measured at Tasiilaq, a coastal station 85 km to the south of Helheim Glacier.

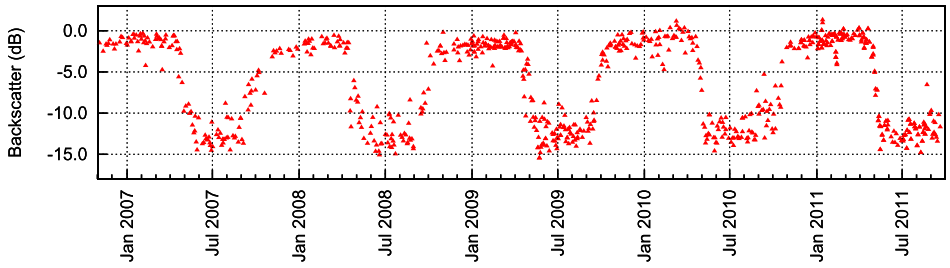

Fig. 3. Backscatter coefficient from Helheim Glacier tongue derived from Envisat ASAR Wide-Swath-Mode (spatial resolution 150 m).

2002). Images were tracked in slant-range geometry with a spatial sampling of 40 m, and multi-looked at 20×20 to a ground pixel size of approximately 40 m. Temporal separation of image pairs used for feature tracking was either 11 days or 22 days. Frontal positions were manually digitised from multi-looked (4×4) SAR intensity images. Errors in the velocity data are estimated to be less than 0.5 m day^{-1} (Bevan et al., 2012).

2.3. GPS bedrock measurements

To estimate site coordinates from GPS measurements, we use the GIPSY OASIS 6.3 software package (Zumberge et al., 1997) developed at the Jet Propulsion Laboratory (JPL) and using IGS orbits, earth orientation parameters, and clock products. The data were processed as described by Khan et al. (2010a) using the Precise Point Positioning (PPP) strategy and the solutions were aligned with the IGS08 frame (Altamimi et al., 2011). To focus on the seasonal mass variability of the Helheim Glacier, we remove the trend, which is due to long-term mass loss over southern portions of Greenland (Khan et al., 2010b). We compare the observed bedrock displacements with predicted displacements obtained by convolving high-resolution spatial seasonal ice volume estimates from the TanDEM-X DEMs (converted to mass change estimates) with the Green's function for vertical displacements derived by Jean-Paul Boy (Petrov and Boy, 2004) for the Preliminary Reference Earth Model (Dziewonski and Anderson, 1981). We convert the seasonal ice volume estimates to mass assuming a density equal to that of ice (917 kg m^{-3}). However, the observed bedrock displacements are caused by mass changes from a greater area than that covered by the DEMs. To include the area outside the DEMs, we estimate ice-sheet-wide seasonal elevation changes during 2003–2009 using Ice, Cloud and land Elevation Satellite (ICESat) laser altimeter data (Zwally et al., 2011b). With this model, overall Greenland mass change matches the GRACE seasonal mass change (Velicogna, 2009).

2.4. Surface melt onset

SAR data are highly sensitive to the presence of meltwater on the glacier surface in the same way that scatterometer data are (e.g. Steffen et al., 2004), backscatter is high when the surface is frozen and low when meltwater is present. Here we use 934 earlier (July 2005 to September 2011) Envisat ASAR Wide-Swath-Mode images to determine typical spring and autumn transitions between surface melt and freeze states at a point approximately 4 km back from the ice front. WSM images have a spatial resolution of 150 m and an acquisition frequency of about 3 days at this latitude (66.4°N). Midday air temperatures from the coastal station of Tasiilaq (85 km to the south of Helheim Glacier) are consistently positive from mid to end April and vary little from year to year (Fig. 2), justifying the use of earlier time series of surface melt to estimate melt onset for the years under consideration in this study.

3. Results

3.1. Elevation changes

A total of 40 DEMs were included in the following analyses with a root mean square (r.m.s.) error relative to the validation point of 1.3 m. The good agreement between DEMs and the validation height gives us high confidence in the DEM differences especially at lower elevations close to the control point where phase unwrapping is initiated. We estimate that SAR penetration depths on the glacier are negligible during the summer following studies that show C-band SAR penetration depths on the Geikie ice cap, just north of Helheim Glacier, to be 0 m in the soaked snow zone between 1600 m and 1900 m (Dall et al., 2001), and 1–2 m on bare ice on Jakobshavn Isbrae, west Greenland (Rignot et al., 2001); the higher frequency X-band TanDEM-X SAR will have a lower penetration depth than C-band SAR. Microwave backscatter values show that melt onset is typically around April or May (Fig. 3) and field studies (Andersen et al., 2010) confirm that the area under consideration in this study, i.e. below 800 m a.m.s.l., is within the ablation zone.

Mapped differences between DEMs (Fig. 4(a)) show that changes are concentrated on the fast-flowing regions of the glacier (Fig. 4(b)). We now calculate elevation changes only where surface flow speeds exceed 1 m day^{-1}. Mean surface elevations, in 100 m elevation bands from 100 m to 800 m a.m.s.l., show annual cycles with a maximum amplitude in 2013 of 19 m between 25/03/2013 and 22/11/2013 in the lowest 100 m elevation band (Fig. 5(a)). Rapid surface lowering begins around July and

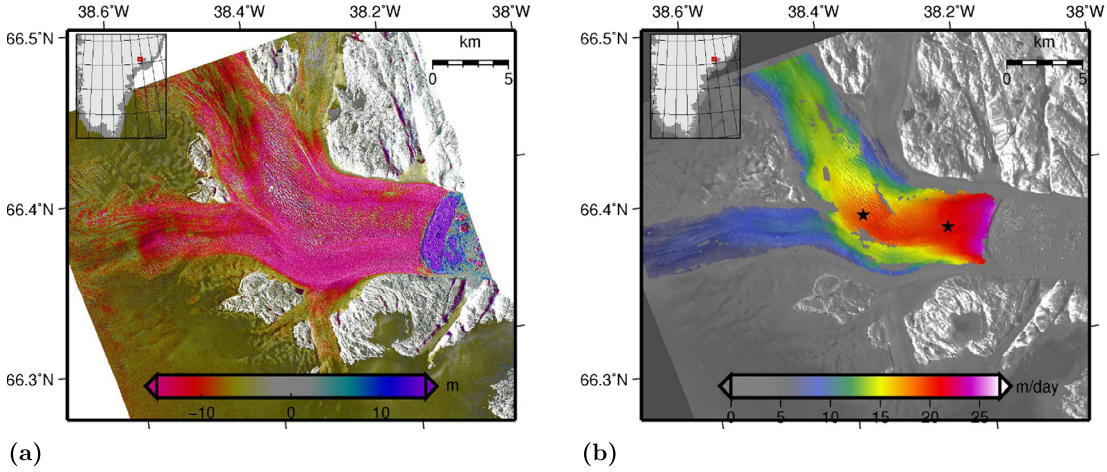

Fig. 4. (a) Map of surface height change from 02/07/2013 to 22/11/2013. The large area of elevation increase at the ice front is where the glacier has advanced. (b) Feature-tracked surface speeds based on images acquired on 24/07/2013 and 04/08/3013. The black stars mark the velocity extraction points.

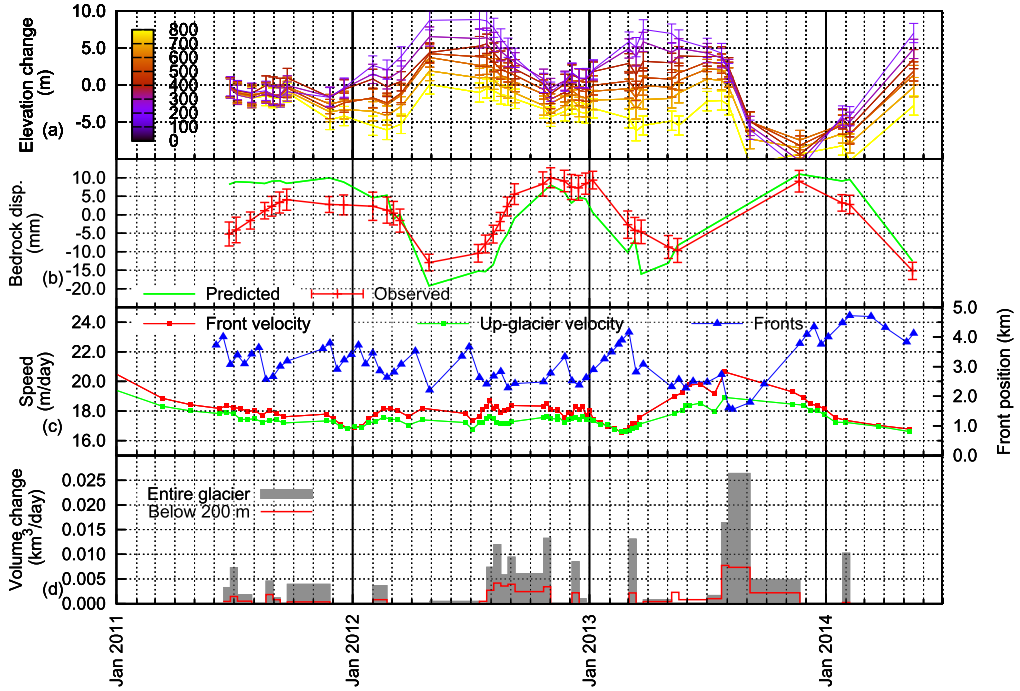

Fig. 5. (a) Time series of mean elevation changes within 100 m altitude bands, from 100 m to 800 m, over fast-flowing (>1 m day^{-1}) areas of the glacier only. Elevation changes are calculated as volume differences relative to the first DEM in the series, on 26/06/2011, divided by the area. Error bars represent ± 1.3 m, the r.m.s. difference between the DEM and the validation height point. (b) Detrended times series of bedrock elevation. The dashed line represents the modelled bedrock response to ice loading and unloading based on the DEM time series, including the factor of 0.7 discussed in the text. (c) Glacier surface velocities extracted at the black stars in Fig. 4(b), and manually digitised frontal positions from along a centre flowline. (d) Water equivalent volume losses between successive DEMs for the entire fast-flowing area of the glacier capture by the DEM coverage.

lasts until October or November. In spite of the quality control applied to DEM selection we see four discontinuities in height change trends in August 2011, February 2012, March 2013 and February 2014. On these occasions we see a reversal of an otherwise monotonic increase or decrease in surface elevation which features in all altitude bands. The jumps are less than 1 m in magnitude and well within our accuracy expectations; they are much less than would be expected from unwrapping errors, as the height of ambiguity is around 48 m, and may therefore be a consequence of errors in satellite orbit information. We include these DEMs in subsequent analyses as we have no objective reason to remove them and also because it is not possible to identify which of two consecutive DEMs contains the error.

3.2. Vertical bedrock displacements

The predicted vertical bedrock displacements, including mass change outside the DEMs (using ice density of 917 kg m^{-3}), are larger than the observed displacements (Fig. 5(b)). The difference between the two curves can be used to estimate an improved density for the volume changes. We obtain a scale of 0.732 ± 0.076 between the two curves, suggesting an improved apparent average density of 671 ± 70 kg m^{-3}. This relatively low ice density indicates that volume changes over the area modelled are a combination of ice, firn and wet snow. In addition, the InSAR DEMs may not resolve all crevasses, so the DEM differences may include air volumes between inter-crevasse ridges, making the bulk density of the measured volume difference even lower. The Pearson's correla-

tion coefficient between the observed and predicted bedrock uplift curves is 0.73, significant at better than 95%.

3.3. Volume losses

Rates of water equivalent volume loss from the fast-flowing area of the glacier captured by the DEMs, that is, entirely below 800 m a.m.s.l., using a glacier surface density of 671 ± 70 kg m^{-3}, peak in August 2013 at 0.026 km^3 day^{-1} (Fig. 5(d)), the total volume for summer 2011 is 0.5 km^3, 2012 is 0.9 km^3 and for 2013 is 1.6 km^3. Generally, up to half of the volume loss originates from elevations below 200 m a.m.s.l. Anomalous spikes in the series, for example in March 2013 and February 2014, occur where there is some positive or negative offset in one of the DEMs used to calculate the change, they can be seen to correspond to the discontinuities in Fig. 5(a).

3.4. Dynamic changes

Throughout the period between June 2011 and May 2014 the velocity close to the front of the glacier (black star in Fig. 4(b)) varies between 16.5 m day^{-1} (February 2013) and 20.6 m day^{-1} (July 2013) (Fig. 5(c)). 5.7 km further up glacier velocities are only slightly lower and follow the same pattern, although the acceleration in 2013 is less pronounced. The ice-front location spans a 3.2 km range, being most advanced in February 2013 and most retreated in August 2013, with calving occurring all year round. There are two periods in the latter half of the record where the glacier advances with little or no calving events and its velocity falls steadily. The first of these periods in early 2013 ends with a 5 month period of retreat and acceleration.

4. Discussion

Elevation changes for Helheim Glacier catchment show a clear seasonal signal, with rapid lowering commencing after July and lasting until October or November. The height change is concentrated on fast-moving (>1 m day^{-1}) areas with no measurable change taking place on the stagnant ice sheet, suggesting that dynamic thinning is a significant contributor to the change. This concentration of height change on the active glacier reflects a similar pattern to the dynamically induced interannual surface lowering observed on Helheim (Pritchard et al., 2009).

A mean Helheim catchment runoff value for 1999–2008 of 1.0 ± 0.2 km^3 yr^{-1} was computed by Mernild et al. (2010) using SnowModel, a snow evolution, ice melt and runoff system model. The runoff was computed over an area of 910 km^2. Our values of 0.5 km^3 yr^{-1} (2011) to 1.6 km^3 yr^{-1} (2013) water equivalent volume change from the 177 km^2 fast-flowing section of the catchment only, indicate that seasonal dynamic effects, resulting in glacier thickness change, are a significant component of Helheim's entire catchment mass balance.

Mass conservation allows temporal thickness changes to be expressed in terms of mass flux divergence and specific mass balance.

$$\frac{\partial S}{\partial t} = b_{sp} - \nabla \cdot (\bar{\mathbf{u}} H) \tag{1}$$

where $\partial S/\partial t$ is the time rate of change of the surface elevation, H is the glacier thickness, b_{sp} the specific mass balance, and u is the depth averaged horizontal velocity vector. The second term on the r.h.s. is the flux divergence.

An attempt to use interpolated grids of glacier thickness supplied by the Center for Remote Sensing of Ice Sheets (CReSIS) to calculate a complete flux divergence field revealed large unrealistic variations. The anomalies are a result of fine-scale features in the velocity field caused by bed topography which is not captured by the sparse flightlines of airborne radar sounding; an effect that has been encountered before, for example on Nioghalvfjerdsfjorden (79 north) Glacier (Seroussi et al., 2011).

Table 1
Summer and winter terms of the flux divergence Equation (2).

	$\partial H/\partial l$	$\bar{u}_l$ (m day^{-1})	$\partial \bar{u}_l/\partial l$ ((m day^{-1})/m)
Summer	0.01	20.6	7.6×10^{-4}
Winter	0.01	17.4	3.9×10^{-4}

However, we can make point estimates of flux divergence using thickness values directly from the CReSIS flightline data, rather than relying on a grid of interpolated values. By considering a winter to summer difference, flux divergence as a result of (unknown) changes in down-flow glacier cross-sectional area cancels out. Treating l as the along-flow direction and with subscripts w and s referring to winter and summer:

$$\nabla \cdot (\bar{\mathbf{u}} H)_{\mathrm{s}} - \nabla \cdot (\bar{\mathbf{u}} H)_{\mathrm{w}} = \left(\frac{\partial (H \bar{u}_l)}{\partial l} \right)_{\mathrm{s}} - \left(\frac{\partial (H \bar{u}_l)}{\partial l} \right)_{\mathrm{w}}. \tag{2}$$

Neglecting temporal changes in thickness and thickness gradient and assuming surface velocities are close to depth averaged velocities, we obtain the values given in Table 1 along a 3834 m section of an along-flow flightline centred on the velocity extraction point, where the ice thickness is 806 m. Winter velocities are from our feature-tracking results for 27/01/2014–07/02/2014 and summer velocities are for 24/07/2013–04/08/2013. From Eq. (2) the increase in flux divergence from winter to summer is approximately 0.33 m day^{-1}, in other words, if $(\partial S/\partial t)_{\mathrm{w}}$ is zero, then $(\partial S/\partial t)_{\mathrm{s}}$ would be -0.33 m day^{-1}.

Thus, the increase in flux divergence from winter to summer on the lower elevations of the glacier is more than sufficient to account for the surface lowering we observe, which is of the order of 0.1 m day^{-1} in summer, without taking any seasonal melt into account. However, there are many assumptions and approximations in the calculation. For example, we do not allow for the probability that flux divergence is a result of crevasse expansion which would not manifest in elevation change, a process that is very likely to be occurring along the lower reaches of the glacier where the stress balance under large velocity gradients will promote crevasse opening and fracture propagation. Our method of calculating elevation change via volume differences between relatively high resolution DEMs may capture some change due to crevasse opening, but some will remain due to unresolved crevasses and due to the SAR DEMs not capturing the full crevasse depth.

We can compare surface elevation changes with field measurements of surface ablation rates. Measurements using sonic-rangers found that ablation rates in 2007 and 2008 on Helheim, at an elevation of 650 m, were of the order of 3.2 cm/day over a 27 day period from the 27th July (Andersen et al., 2010). Over the whole melt period and between 600 m and 700 m, we observe a mean rate of thinning of 6.5 cm/day in 2013, and 5.0 cm/day in 2012. At Tasiilaq in 2007 there were 198 positive degree days (PDDs) and in 2013 there were only 165 (Fig. 2); use of a PDD model to determine surface melt would indicate that surface melt in 2013 was less than 2007. The additional surface lowering we observe is, therefore, most likely due to dynamic thinning (which would not be measured with the sonic-ranger method) plus any basal melt.

The seasonal dynamic effects are more clearly observed in the time series and maps of surface elevation change than in glacier surface velocity; only from July 2013, when glacier thinning was most pronounced, do we observe a clear increase in flow speed which precedes the thinning. The record of flow speeds presented here continues that in Bevan et al. (2012) which showed that an-

nual peaks in velocity are common but not observed in every year. Whether seasonal velocity increases on outlet glaciers occur because of basal lubrication following meltwater penetration to the bed or because of ice-front retreat changing the force balance at the terminus is still unresolved.

Although surface melting can have a significant impact on ice-sheet flow (Zwally et al., 2002; Joughin et al., 2008; Das et al., 2008; Palmer et al., 2011), the net impact on the dynamics of outlet glaciers of enhanced seasonal melt is usually found to be small, i.e. less than 15% (Joughin et al., 2008). Meltwater has been observed to briefly accelerate flow but the development of a more efficient subglacial drainage system, as melt volumes increase, can subsequently cause abrupt slow down (Howat et al., 2010), resulting in a very small overall increase in annual flow speed (Sole et al., 2011). Brief speed-ups have been observed to follow episodes of enhanced surface melting on Helheim (Andersen et al., 2010), but are less significant than those following calving episodes (Nettles et al., 2008; Sundal et al., 2013). However, whereas seasonal changes in front position are found to influence flow speeds for accelerating and retreating glaciers (Nick et al., 2009) such as Jakobshavn Isbrae in west Greenland (Joughin et al., 2008), they do not appear to have a dominant influence on the dynamics of stable outlet glaciers (Howat et al., 2010).

In this instance, whilst we see a clear signal of dynamic origin in the glacier surface elevation, we do not observe a corresponding signal in the ice-front position; in fact, from August 2013 when the glacier is thinning the ice front is advancing. It therefore seems most likely that it is surface melt, penetrating to the bed, which causes the dynamic component of glacier seasonal thinning rather than any acceleration as a result of changes in back stress at the glacier terminus.

4.1. Conclusions

Long-term mass-balance trends on the Greenland Ice Sheet are driven by disruptions to the seasonal mass balance cycle; understanding the seasonal cycle, especially on fast-flowing marine-terminating glaciers, underpins any attempt to predict long-term mass loss. We investigated three full years of seasonal mass-balance cycles on Helheim Glacier in south-east Greenland using bedrock GPS measurements and a series of 40 TanDEM-X interferometric digital elevation models (DEMs).

We conclude that seasonal mass loss by dynamic thinning is of the same order of magnitude as our observed decreases in surface elevation and that, on the basis of ice-front position observations through the time series, melt-induced acceleration is most likely the main driver of the thinning, as opposed to changes triggered at the terminus.

The calculation of large-scale flux divergence quantities, which would enable more precise estimates of the glacier-wide dynamic component of thinning, was found to require a much finer resolution ice-thickness grid than is currently available. The magnitude of seasonal changes in ice-surface elevations highlights the importance of selecting consistent measurement dates when using altimetry to assess long-term temporal change in glacier thickness.

Acknowledgements

S. Bevan was supported by the Welsh Institute for Sustainable Environments (WISE) and the Climate Change Consortium for Wales (C3W), and is currently employed on NERC project NE/L005409/1. S.A. Khan was partly supported by KVUG (11-104050) and the Danish Council for Independent Research – Nature and Universe (12-125118). TanDEM-X data were supplied by DLR, as part of NERC project NE/I00714811. We acknowledge the use of data products from CReSIS generated with support from NSF grant ANT-0424589 and NASA grant NNX10AT68G. Thanks to the Danish Meteorological Institute for Tasiilaq air temperature data and to Alistair Everett for help with the manuscript.

References

Ahlstrøm, A.P., Andersen, S.B., Andersen, M.L., Machguth, H., Nick, F.M., Joughin, I., Reijmer, C.H., van de Wal, R.S.W., Merryman Boncori, J.P., Box, J.E., Citterio, M., van As, D., Fausto, R.S., Hubbard, A., 2013. Seasonal velocities of eight major marine-terminating outlet glaciers of the Greenland ice sheet from continuous in situ GPS instruments. Earth Syst. Sci. Data 5, 277–287. http://dx.doi.org/10.5194/essd-5-277-2013.

Altamimi, Z., Collilieux, X., Métivier, L., 2011. ITRF2008: an improved solution of the international terrestrial reference frame. J. Geod. 85, 457–473. http://dx.doi.org/10.1007/s00190-011-0444-4.

Amundson, J.M., Fahnestock, M., Truffer, M., Brown, J., Lüthi, M.P., Motyka, R.J., 2010. Ice mélange dynamics and implications for terminus stability, Jakobshavn Isbræ, Greenland. J. Geophys. Res. 115, F01005+. http://dx.doi.org/10.1029/2009jf001405.

Andersen, M.L., Larsen, T.B., Nettles, M., Elosegui, P., van As, D., Hamilton, G.S., Stearns, L.A., Davis, J.L., Ahlstrøm, A.P., de Juan, J., Ekström, G., Stenseng, L., Khan, S.A., Forsberg, R., Dahl-Jensen, D., 2010. Spatial and temporal melt variability at Helheim Glacier, East Greenland, and its effect on ice dynamics. J. Geophys. Res. 115. http://dx.doi.org/10.1029/2010jf001760.

Bamber, J., van den Broeke, M., Ettema, J., Lenaerts, J., Rignot, E., 2012. Recent large increases in freshwater fluxes from Greenland into the North Atlantic. Geophys. Res. Lett. 39, L19501+. http://dx.doi.org/10.1029/2012gl052552.

Bartholomew, I., Nienow, P., Mair, D., Hubbard, A., King, M.A., Sole, A., 2010. Seasonal evolution of subglacial drainage and acceleration in a Greenland outlet glacier. Nat. Geosci. 3, 408–411. http://dx.doi.org/10.1038/ngeo863.

Bartholomew, I., Nienow, P., Sole, A., Mair, D., Cowton, T., Palmer, S., Wadham, J., 2011. Supraglacial forcing of subglacial drainage in the ablation zone of the Greenland ice sheet. Geophys. Res. Lett. 38, L08502+. http://dx.doi.org/10.1029/2011gl047063.

Bevan, S.L., Luckman, A.J., Murray, T., 2012. Glacier dynamics over the last quarter of a century at Helheim, Kangerdlugssuaq and 14 other major Greenland outlet glaciers. Cryosphere 6, 923–937. http://dx.doi.org/10.5194/tc-6-923-2012.

Bevis, M., Wahr, J., Khan, S.A., Madsen, F.B., Brown, A., Willis, M., Kendrick, E., Knudsen, P., Box, J.E., van Dam, T., Caccamise, D.J., Johns, B., Nylen, T., Abbott, R., White, S., Miner, J., Forsberg, R., Zhou, H., Wang, J., Wilson, T., Bromwich, D., Francis, O., 2012. Bedrock displacements in Greenland manifest ice mass variations, climate cycles and climate change. Proc. Natl. Acad. Sci. USA 109, 11944–11948. http://dx.doi.org/10.1073/pnas.1204664109.

van den Broeke, M., Bamber, J., Ettema, J., Rignot, E., Schrama, E., Van de Berg, W.J., Van Meijgaard, E., Velicogna, I., Wouters, B., 2009. Partitioning recent Greenland mass loss. Science 326, 984–986. http://dx.doi.org/10.1126/science.1178176.

Chen, J.L., Wilson, C.R., Tapley, B.D., 2006. Satellite gravity measurements confirm accelerated melting of Greenland Ice Sheet. Science 313, 1958–1960. http://dx.doi.org/10.1126/science.1129007.

Clason, C.C., Mair, D.W.F., Nienow, P.W., Bartholomew, I.D., Sole, A., Palmer, S., Schwanghart, W., 2014. Modelling the transfer of supraglacial meltwater to the bed of Leverett Glacier, southwest Greenland. Cryosph. Discuss. 8, 4243–4280. http://dx.doi.org/10.5194/tcd-8-4243-2014.

Cook, S., Rutt, I.C., Murray, T., Luckman, A., Zwinger, T., Selmes, N., Goldsack, A., James, T.D., 2014. Modelling environmental influences on calving at Helheim Glacier in eastern Greenland. Cryosphere 8, 827–841. http://dx.doi.org/10.5194/tc-8-827-2014.

Cook, S., Zwinger, T., Rutt, I.C., O'Neel, S., Murray, T., 2012. Testing the effect of water in crevasses on a physically based calving model. Ann. Glaciol. 53 (60), 90–96. http://dx.doi.org/10.3189/2012aog60a107.

Dall, J., Madsen, S.N., Keller, K., Forsberg, R., 2001. Topography and penetration of the Greenland Ice Sheet measured with Airborne SAR Interferometry. Geophys. Res. Lett. 28. http://dx.doi.org/10.1029/2000gl011787.

Das, S.B., Joughin, I., Behn, M.D., Howat, I.M., King, M.A., Lizarralde, D., Bhatia, M.P., 2008. Fracture propagation to the base of the Greenland Ice Sheet during Supraglacial Lake drainage. Science 320, 778–781. http://dx.doi.org/10.1126/science.1153360.

Dziewonski, A.M., Anderson, D.L., 1981. Preliminary reference Earth model. Phys. Earth Planet. Inter. 25, 297–356. http://dx.doi.org/10.1016/0031-9201(81)90046-7.

Ewert, H., Groh, A., Dietrich, R., 2012. Volume and mass changes of the Greenland ice sheet inferred from ICESat and GRACE. J. Geodyn. 59–60, 111–123. http://dx.doi.org/10.1016/j.jog.2011.06.003.

Farrell, W.E., 1972. Deformation of the Earth by surface loads. Rev. Geophys. 10, 761–797. http://dx.doi.org/10.1029/rg010i003p00761.

Helm, V., Humbert, A., Miller, H., 2014. Elevation and elevation change of Greenland and Antarctica derived from Cryosat-2. Cryosphere 8, 1539–1559. http://dx.doi.org/10.5194/tc-8-1539-2014.

Howat, I.M., Ahn, Y., Joughin, I., van den Broeke, M.R., Lenaerts, J.T.M., Smith, B., 2011. Mass balance of Greenland's three largest outlet glaciers, 20002010. Geophys. Res. Lett. 38, L12501+. http://dx.doi.org/10.1029/2011gl047565.

Howat, I.M., Box, J.E., Ahn, Y., Herrington, A., McFadden, E.M., 2010. Seasonal variability in the dynamics of marine-terminating outlet glaciers in Greenland. J. Glaciol. 56 (198), 601–613. http://dx.doi.org/10.3189/002214310793146232.

Howat, I.M., Joughin, I., Scambos, T.A., 2007. Rapid changes in ice discharge from Greenland Outlet glaciers. Science 315, 1559–1561. http://dx.doi.org/10.1126/science.1138478.

Howat, I.M., Joughin, I., Tulaczyk, S., Gogineni, S., 2005. Rapid retreat and acceleration of Helheim Glacier, east Greenland. Geophys. Res. Lett. 32, L22502+. http://dx.doi.org/10.1029/2005gl024737.

Jenkins, A., 2011. Convection-driven melting near the grounding lines of ice shelves and tidewater glaciers. J. Phys. Oceanogr. 41, 2279–2294. http://dx.doi.org/10.1175/jpo-d-11-03.1.

Johannessen, O.M., Khvorostovsky, K., Miles, M.W., Bobylev, L.P., 2005. Recent ice-sheet growth in the interior of Greenland. Science 310, 1013–1016. http://dx.doi.org/10.1126/science.1115356.

Joughin, I., Das, S.B., King, M.A., Smith, B.E., Howat, I.M., Moon, T., 2008. Seasonal speedup along the western flank of the Greenland ice sheet. Science 320, 781–783. http://dx.doi.org/10.1126/science.1153288.

Khan, S.A., Kjaer, K.H., Bevis, M., Bamber, J.L., Wahr, J., Kjeldsen, K.K., Bjork, A.A., Korsgaard, N.J., Stearns, L.A., van den Broeke, M.R., Liu, L., Larsen, N.K., Muresan, I.S., 2014. Sustained mass loss of the northeast Greenland ice sheet triggered by regional warming. Nat. Clim. Change 4, 292–299. http://dx.doi.org/10.1038/nclimate2161.

Khan, S.A., Liu, L., Wahr, J., Howat, I., Joughin, I., van Dam, T., Fleming, K., 2010a. GPS measurements of crustal uplift near Jakobshavn Isbræ due to glacial ice mass loss. J. Geophys. Res. 115, B09405+. http://dx.doi.org/10.1029/2010jb007490.

Khan, S.A., Wahr, J., Bevis, M., Velicogna, I., Kendrick, E., 2010b. Spread of ice mass loss into northwest Greenland observed by GRACE and GPS. Geophys. Res. Lett. 37. http://dx.doi.org/10.1029/2010gl042460.

Krabill, W., Abdalati, W., Frederick, E., Manizade, S., Martin, C., Sonntag, J., Swift, R., Thomas, R., Wright, W., Yungel, J., 2000. Greenland ice sheet: high-elevation balance and peripheral thinning. Science 289, 428–430.

Krabill, W., Frederick, E., Manizade, S., Martin, C., Sonntag, J., Swift, R., Thomas, R., Wright, W., Yungel, J., 1999. Rapid thinning of parts of the southern Greenland Ice Sheet. Science 283, 1522–1524. http://dx.doi.org/10.1126/science.283.5407.1522.

Krieger, G., Zink, M., Bachmann, M., Bräutigam, B., Schulze, D., Martone, M., Rizzoli, P., Steinbrecher, U., Walter Antony, J., De Zan, F., Hajnsek, I., Papathanassiou, K., Kugler, F., Rodriguez Cassola, M., Younis, M., Baumgartner, S., López-Dekker, P., Prats, P., Moreira, A., 2013. TanDEM-X: a radar interferometer with two formation-flying satellites. Acta Astronaut. 89, 83–98. http://dx.doi.org/10.1016/j.actaastro.2013.03.008.

Luckman, A., Murray, T., de Lange, R., Hanna, E., 2006. Rapid and synchronous ice-dynamic changes in East Greenland. Geophys. Res. Lett. 33. http://dx.doi.org/10.1029/2005gl025428.

Mernild, S.H., Howat, I.M., Ahn, Y., Liston, G.E., Steffen, K., Jakobsen, B.H., Hasholt, B., Fog, B., van As, D., 2010. Freshwater flux to Sermilik Fjord, se Greenland. Cryosphere 4, 453–465. http://dx.doi.org/10.5194/tc-4-453-2010.

Motyka, R.J., Hunter, L., Echelmeyer, K.A., Connor, C., 2003. Submarine melting at the terminus of a temperate tidewater glacier, LeConte Glacier, Alaska, U.S.A. Ann. Glaciol. 36, 57–65. http://dx.doi.org/10.3189/172756403781816374.

Murray, T., Scharrer, K., James, T.D., Dye, S.R., Hanna, E., Booth, A.D., Selmes, N., Luckman, A., Hughes, A.L.C., Cook, S., Huybrechts, P., 2010. Ocean regulation hypothesis for glacier dynamics in southeast Greenland and implications for ice sheet mass changes. J. Geophys. Res. 115. http://dx.doi.org/10.1029/2009jf001522.

Nettles, M., Larsen, T.B., Elósegui, P., Hamilton, G.S., Stearns, L.A., Ahlstrøm, A.P., Davis, J.L., Andersen, M.L., de Juan, J., Khan, S.A., Stenseng, L., Ekström, G., Forsberg, R., 2008. Step-wise changes in glacier flow speed coincide with calving and glacial earthquakes at Helheim Glacier, Greenland. Geophys. Res. Lett. 35, L24503+. http://dx.doi.org/10.1029/2008gl036127.

Nick, F.M., Vieli, A., Howat, I.M., Joughin, I., 2009. Large-scale changes in Greenland outlet glacier dynamics triggered at the terminus. Nat. Geosci. 2, 110–114. http://dx.doi.org/10.1038/ngeo394.

Nielsen, K., Khan, S.A., Spada, G., Wahr, J., Bevis, M., Liu, L., van Dam, T., 2013. Vertical and horizontal surface displacements near Jakobshavn Isbræ driven by melt-induced and dynamic ice loss. J. Geophys. Res., Solid Earth 118, 1837–1844. http://dx.doi.org/10.1002/jgrb.50145.

O'Leary, M., Christoffersen, P., 2013. Calving on tidewater glaciers amplified by submarine frontal melting. Cryosphere 7, 119–128. http://dx.doi.org/10.5194/tc-7-119-2013.

Palmer, S., Shepherd, A., Nienow, P., Joughin, I., 2011. Seasonal speedup of the Greenland Ice Sheet linked to routing of surface water. Earth Planet. Sci. Lett. http://dx.doi.org/10.1016/j.epsl.2010.12.037.

Petrov, L., Boy, J.P., 2004. Study of the atmospheric pressure loading signal in very long baseline interferometry observations. J. Geophys. Res. 109, B03405+. http://dx.doi.org/10.1029/2003jb002500.

Pritchard, H.D., Arthern, R.J., Vaughan, D.G., Edwards, L.A., 2009. Extensive dynamic thinning on the margins of the Greenland and Antarctic ice sheets. Nature 461, 971–975. http://dx.doi.org/10.1038/nature08471.

Rignot, E., Box, J.E., Burgess, E., Hanna, E., 2008. Mass balance of the Greenland ice sheet from 1958 to 2007. Geophys. Res. Lett. 35, L20502+. http://dx.doi.org/10.1029/2008gl035417.

Rignot, E., Echelmeyer, K., Krabill, W., 2001. Penetration depth of interferometric synthetic-aperture radar signals in snow and ice. Geophys. Res. Lett. 28, 3501–3504. http://dx.doi.org/10.1029/2000gl012484.

Rignot, E., Kanagaratnam, P., 2006. Changes in the velocity structure of the Greenland ice sheet. Science 311, 986–990. http://dx.doi.org/10.1126/science.1121381.

Sciascia, R., Straneo, F., Cenedese, C., Heimbach, P., 2013. Seasonal variability of submarine melt rate and circulation in an East Greenland fjord. J. Geophys. Res., Oceans. http://dx.doi.org/10.1002/jgrc.20142.

Seroussi, H., Morlighem, M., Rignot, E., Larour, E., Aubry, D., Dhia, H.B., Kristensen, S.S., 2011. Ice flux divergence anomalies on 79north Glacier, Greenland. Geophys. Res. Lett. 38, L09501+. http://dx.doi.org/10.1029/2011gl047338.

Shepherd, A., Ivins, E.R., Geruo Barletta, V.R., Bentley, M.J., Bettadpur, S., Briggs, K.H., Bromwich, D.H., Forsberg, R., Galin, N., Horwath, M., Jacobs, S., Joughin, I., King, M.A., Lenaerts, J.T.M., Li, J., Ligtenberg, S.R.M., Luckman, A., Luthcke, S.B., McMillan, M., Meister, R., Milne, G., Mouginot, J., Muir, A., Nicolas, J.P., Paden, J., Payne, A.J., Pritchard, H., Rignot, E., Rott, H., Sørensen, L.S., Scambos, T.A., Scheuchl, B., Schrama, E.J.O., Smith, B., Sundal, A.V., van Angelen, J.H., van de Berg, W.J., van den Broeke, M.R., Vaughan, D.G., Velicogna, I., Wahr, J., Whitehouse, P.L., Wingham, D.J., Yi, D., Young, D., Zwally, H.J., 2012. A reconciled estimate of ice-sheet mass balance. Science 338, 1183–1189. http://dx.doi.org/10.1126/science.1228102.

Sole, A.J., Mair, D.W.F., Nienow, P.W., Bartholomew, I.D., King, M.A., Burke, M.J., Joughin, I., 2011. Seasonal speedup of a Greenland marine-terminating outlet glacier forced by surface meltinduced changes in subglacial hydrology. J. Geophys. Res. 116, F03014+. http://dx.doi.org/10.1029/2010jf001948.

Stearns, L.A., Hamilton, G.S., 2007. Rapid volume loss from two East Greenland outlet glaciers quantified using repeat stereo satellite imagery. Geophys. Res. Lett. 34, L05503+. http://dx.doi.org/10.1029/2006gl028982.

Steffen, K., Nghiem, S.V., Huff, R., Neumann, G., 2004. The melt anomaly of 2002 on the Greenland Ice Sheet from active and passive microwave satellite observations. Geophys. Res. Lett. 31, L20402+. http://dx.doi.org/10.1029/2004gl020444.

Strozzi, T., Luckman, A., Murray, T., Wegmüller, U., Werner, C.L., 2002. Glacier motion estimation using SAR offset-tracking procedures. IEEE Trans. Geosci. Remote Sens. 40, 2384–2391.

Sundal, A.V., Shepherd, A., Van Den Broeke, M., Van Angelen, J., Gourmelen, N., Park, J., 2013. Controls on short-term variations in Greenland glacier dynamics. J. Glaciol. 59 (217), 883–892. http://dx.doi.org/10.3189/2013jog13j019.

Sutherland, D.A., Straneo, F., Pickart, R.S., 2014. Characteristics and dynamics of two major Greenland glacial fjords. J. Geophys. Res., Oceans 119, 3767–3791. http://dx.doi.org/10.1002/2013jc009786.

Thomas, R., Frederick, E., Krabill, W., Manizade, S., Martin, C., 2006. Progressive increase in ice loss from Greenland. Geophys. Res. Lett. 33, L10503+. http://dx.doi.org/10.1029/2006gl026075.

Velicogna, I., 2009. Increasing rates of ice mass loss from the Greenland and Antarctic ice sheets revealed by GRACE. Geophys. Res. Lett. 36. http://dx.doi.org/10.1029/2009gl040222.

Velicogna, I., Wahr, J., 2005. Greenland mass balance from GRACE. Geophys. Res. Lett. 32. http://dx.doi.org/10.1029/2005gl023955.

Wahr, J., Khan, S.A., van Dam, T., Liu, L., van Angelen, J.H., van den Broeke, M.R., Meertens, C.M., 2013. The use of GPS horizontals for loading studies, with applications to northern California and southeast Greenland. J. Geophys. Res., Solid Earth 118, 1795–1806. http://dx.doi.org/10.1002/jgrb.50104.

Zumberge, J.F., Heflin, M.B., Jefferson, D.C., Watkins, M.M., Webb, F.H., 1997. Precise point positioning for the efficient and robust analysis of GPS data from large networks. J. Geophys. Res. 102, 5005–5017. http://dx.doi.org/10.1029/96jb03860.

Zwally, H.J., Abdalati, W., Herring, T., Larson, K., Saba, J., Steffen, K., 2002. Surface melt-induced acceleration of Greenland Ice-Sheet flow. Science 297, 218–222. http://dx.doi.org/10.1126/science.1072708.

Zwally, H.J., Li, J., Brenner, A.C., Beckley, M., Cornejo, H.G., Dimarzio, J., Giovinetto, M.B., Neumann, T.A., Robbins, J., Saba, J.L., Yi, D., Wang, W., 2011a. Greenland ice sheet mass balance: distribution of increased mass loss with climate warming; 2003–07 versus 1992–2002. J. Glaciol. 57, 88–101. http://www.igsoc.org/journal/57/201/j10j101.pdf.

Zwally, H.J., Schutz, R., Bentley, C., Bufton, J., Herring, T., Minster, J., Spinhirne, J., Thomas, R., 2011b. GLAS/ICESat L2 Antarctic and Greenland Ice Sheet altimetry data V031. NASA Distributed Active Archive Center at the National Snow and Ice Data Center, Digital Media, Boulder, Colorado.